Technium Vol. 13, pp.88-101 (2023)
ISSN: 2668-778X
www.techniumscience.com

Structural, electronic, linear, and nonlinear optical properties of undoped and Mo (I, II)-doped $LiNbO_3$ crystal

W. A. Abdul-Hussein[1*], and A. J. Almusawe[2]

[1]Department of Science, College of Basic Education, University of Sumer, 64005, Rifaee, IRAQ

[2]Department of Physics, College of Science, University of Basrah, 61004, Basrah, IRAQ

[*]Corresponding Author, w.a.abdulhussein@uos.edu.iq

Abstract. In this paper, density functional theory (DFT) calculations used to investigate the structural, electronic, linear and nonlinear optical properties of pure lithium niobate crystal ($LiNbO_3$) and doped $LiNbO_3$ by Mo (I) and Mo (I). The lattice constants were calculated by analysing the optimised unit cell, and the results were found to be in good agreement with both the experimental and theoretical values that were reported. The results indicate a clear distinction in the electronic characteristics of $LiNbO_3$ and doped $LiNbO_3$ (Mo-Nb), the band structures that have been computed indicate that the band gap of $LiNbO_3$ can be narrowed by adding Mo (I) and Mo (II) dopants to 2.068 eV and 0.476 eV, respectively. Interesting results were obtained by this doping process, as these results showed that the effect of doping led to an improvement in some optical properties, such as the absorption spectrum of the material, and also led to an increase in the effect of second harmonic generation (SHG), which is considered a basic requirement for developing optical devices in many photonic applications such as laser, electro-optic applications and optical switches.

Keyword: First Principles, Molybdenum doping, $LiNbO_3$, Electronic characteristics; Optical characteristics.

Introduction

An important family of second-order nonlinear optical materials are inorganic crystals. Additionally, it is frequently researched for a variety of photonic applications, such as resonators, filters, electro-optic, sensors, and SHG [1-3]. Due to its exceptional piezoelectric and photonic performances, the lithium-niobate (LN) is extensively utilized in commercial piezoelectric crystal materials. The LN

crystal has 3 m symmetry and belongs to the trigonal crystal system. The ferroelectric substance LN has a layered structure. Because of its superior ferroelectric, photorefractive, electro-optic, piezoelectric, and photocatalytic properties as well as its rapid electro optical response (> 100 GHz) and broad transparency window between 0.4 and 4.5 m wavelengths, it has generated a lot of interest as a potential functional material [4-9]. These materials exhibit phase transitions of second order or those that closely resemble second-order transitions. They maintain uniaxial characteristics over all temperature ranges, with a sole structural phase transition that aligns with the Curie temperature. The lattice dynamical representation of these systems is complicated by the presence of intricate optical modes of lattice vibration, which can be attributed to the high Curie temperature exhibited by $LiNbO_3$ (1200 C). [5, 7, 8]. $LiNbO_3$ is an ABO_3 lattice even though it lacks the perovskite structure, with adjacent oxygen octahedral BO_6 sharing common faces. This substance holds significant importance due to its exceptional quality as a source material, characterized by little optical loss. Integrated optics comprising lasers, filters, and modulators on just a single $LiNbO_3$ substrate demonstrate considerable potential. Furthermore, the progression of laser technology and optical communications necessitates the use of materials that possess substantial nonlinear optical and electro-optic reactions [10-13]. It is commonly known that materials with a large linear behavior can also reach large nonlinear polarizability**.** This paper reports the theoretical study of structural, electronic and linear-nonlinear optical properties of pure and doped $LiNbO_3$ crystals. It is important to get additional data about the substance due to its unique and distinctive physical features. One of the most advanced methods for examining a material's various properties in condensed matter physics is DFT. In light of this, the structural, electronic, and optical characteristics of $LiNbO_3$ have been examined in the current work utilizing DFT.

Computational details and Structural properties

The computations of $LiNbO_3$ and doped $LiNbO_3$ by Mo (I) and Mo (II) were performed using the DFT method, applying the SIESTA ab initio simulation package [14, 15]. The exchange-correlation potential in this study is determined using the Perdew, Burke, and Ernzerhof (PBE) functional scheme [16], which is a generalized gradient approximation (GGA) method. The investigation has focused on the convergence tests of the total energy with a cut-off energy of 150 hartrees, and the energy convergence criteria were met at a threshold of 1×10^{-5} eV. The k-point grids are configured according to the Monkhorst−Pack scheme [17], specifically as a 16×16×1 grid, at a temperature of 300 K. The crystal structure of pure and doped $LiNbO_3$ are shown below in Fig. 1 and the Lattice parameters of these crystal structures are provided in Table 1.

Technium Vol. 13, pp.88-101 (2023)
ISSN: 2668-778X
www.techniumscience.com

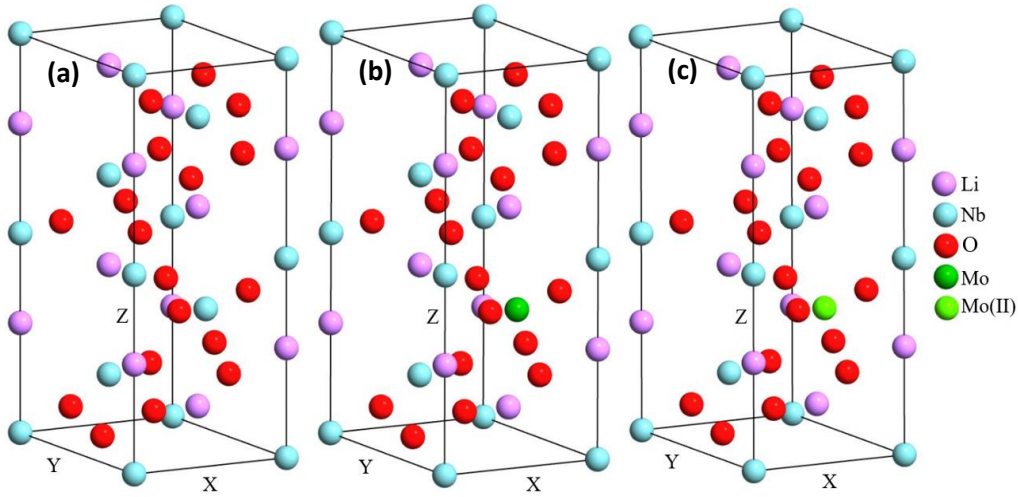

Figure 1. The schematic crystal structure of (a) $LiNbO_3$, (b) Li(Nb-Mo I)O_3, and (c) Li(Nb-Mo II)O_3.

Results and discussion

Structural properties

Optimizations are performed on individual supercells in order to mitigate external pressures. This leads to the formation of less strained crystal lattices in $LiNbO_3$, and the optimization of energy versus volume yields equilibrium lattice parameters in both scenarios. The lattice parameters for the $LiNbO_3$ system were determined to be a=b=5.1502 Å and c=13.8653 Å, respectively. These values exhibit a high level of agreement with the experimental lattice parameters of a=b=5.147 Å and c=13.849 Å reported in a previous study [18], as well as with the findings of previous first principles investigations, which reported a value of a=b=5.057 Å and c=13.942 Å [19]. Table 1 presents the lattice characteristics of LiNbO3 before and after the introduction of Mo (I, II) doping. Lattice parameter is a significant parameter that is associated with the gap, as the electronic band gap is contingent upon the transition between cations and anions, hence relying on the interatomic distance separating them.

Table 1. Lattice parameters of undoped and Mo (I, II)-doped $LiNbO_3$ system.

Lattice parameters	a (Å)	b (Å)	c (Å)	α	β	γ
$LiNbO_3$	5.1502	5.1502	13.8653	90.0000	90.0000	120.0000
Li(Nb, Mo)O_3	5.2705	5.2706	14.2311	90.0086	89.9912	120.0430
Li(Nb, Mo II)O_3	5.4150	5.3446	14.4148	87.0810	91.6866	119.9550

Technium Vol. 13, pp.88-101 (2023)
ISSN: 2668-778X
www.techniumscience.com

In addition, when Mo (I, II) is replaced by Nb atom, the bond lengths between ($O_{18,19,20,\ 27,\ 28,\ 29}$–Mo (I)), ($O_{18,19,20,\ 27,\ 28,\ 29}$–Mo (II)), and ($O_{18,19,20,\ 27,\ 28,\ 29}$–Nb) in pure structure, were determined and are presented in Table 2.

Table 2. Octahedron parameters of undoped and Mo (I, II)-doped $LiNbO_3$ system.

	Nb-O octahedron (LiNbO3)	Mo-O octahedron ($LiNb_{5/6}$ $Mo_{1/6}O3$)	Mo (II)-O octahedron ($LiNb_{4/6}$ $Mo_{1/6}O3$)
Bond length (Å)	Nb-O_{18}=1.84377	Mo-O_{18}=1.97000	Mo-O_{18}=1.90494
	Nb-O_{19}=1.84377	Mo -O_{19}=1.97262	Mo -O_{19}=1.84825
	Nb-O_{20}=1.84377	Mo -O_{20}=1.96912	Mo –O_{20}=1.89468
	Nb-O_{27}=2.17923	Mo -O_{27}=2.10026	Mo -O_{27}=2.14854
	Nb-O_{28}=2.17923	Mo -O_{28}=2.10131	Mo -O_{28}=2.16291
	Nb-O_{29}=2.17923	Mo -O_{29}=2.10242	Mo -O_{29}=2.15138
Average bond length (Å)	2.01150	2.03596	2.01845

Electronic properties

The term "band gap" pertains to the difference in energy levels between the lowest and highest energy state within the conduction band (CB) and the valence band (VB), respectively. This phenomenon is commonly referred to as the energy gap, and it plays a crucial role in comprehending the conductivity characteristics of a certain material. This phenomenon is commonly referred to as the energy band gap in solid materials, wherein electrons exhibit limited longevity. When the VB reaches its maximum and the CB reaches its minimum along the same energy line, it is referred to as direct band gap. Otherwise, when the maximum of VB and the minimum of CB occur at different energy levels, it is known as an indirect band gap [20]. The analysis of the band structure is crucial for obtaining insights into the potential energy ranges available for both occupied and unoccupied electrons, as well as understanding the transitions of electrons from VB to the CB. Fig. 2 (a) depicts the band structure and density of states (DOS) of $LiNbO_3$. The VB exhibits its maximum intensity at the G point, while the CB displays its minimum intensity at the U point. The disparity between these two energy levels is measured to be indirect band gap of 3.538 eV. The band gap exhibits a close proximity to the experimental value as reported in previous studies [21-23]. Due to the indirect character of the band gap, a significant portion of the incident energy is dissipated as electrons migrate from VB to CB. Fig. 2 (b) depicts the band structure of $LiNbO_3$ doped with (Nb-Mo I). The CB has peaks that are not coincident with the minima of the VB, hence indicating the indirect character of the band gap. The VB exhibits its maximum at the

Z point, while the CB displays its minimum at the V point, leading to gap of 2.068 eV. The findings indicate a decrease in gap when comparing it to the band gap of $LiNbO_3$. Therefore, the presence of a characteristic band gap in semiconductors was found subsequent to the process of doping. In Fig. 2 (c), the determined band gap value of $LiNbO_3$ doped with (Nb-Mo II) is recorded as 0.476 eV, indicating a significantly reduced magnitude compared to the band gap value of pristine $LiNbO_3$.

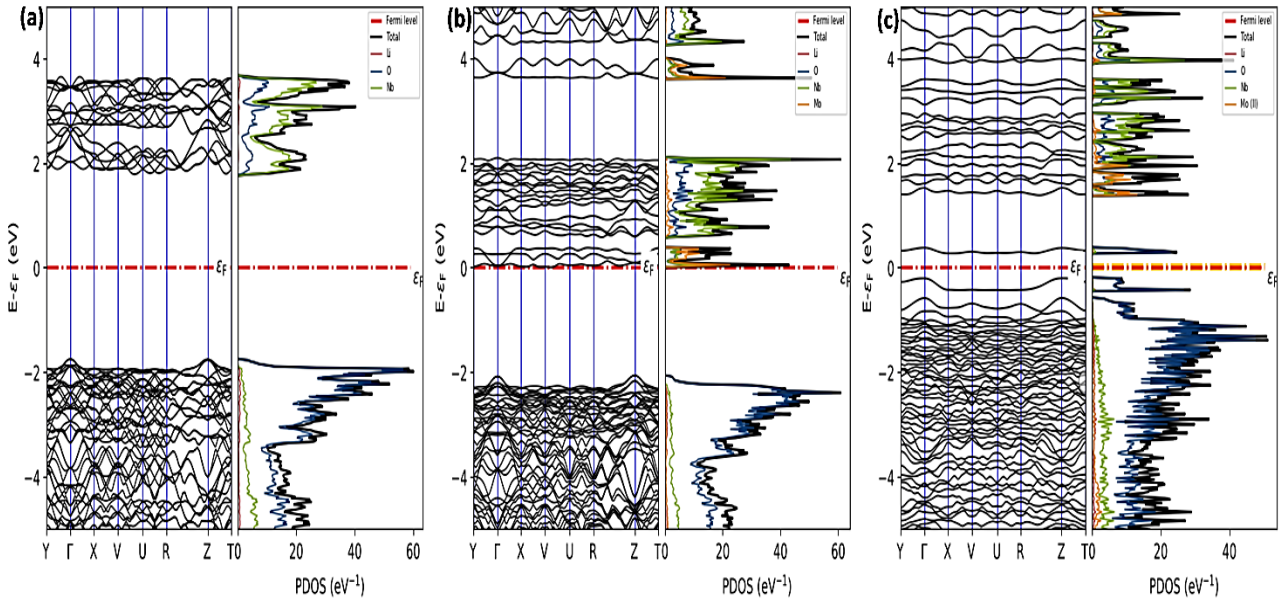

Figure 2. Band structure and DOS of (a) $LiNbO_3$ (b) Li(Nb-Mo I)O_3 (c) Li(Nb-Mo II)O_3.

Optical properties

The investigation of the optical characteristics of substances holds significant relevance in numerous electronic and optical applications, such as solar cells and light-emitting diodes. This is due to its ability to provide a comprehensive understanding of the material's response to external electromagnetic radiation, hence offering valuable insights into its behavior [24-26].

This study investigates the linear optical properties, which include absorption coefficient, refractive index, reflectivity, dielectric constant, polarization, and optical conductivity, as well as the nonlinear optical properties, specifically SHG, in pure and doped LiNbO3 crystals. The investigation covers incident radiation energies up to 20 eV, as depicted in the below figures. That can be determined by the utilization of the frequency-dependent dielectric function $\varepsilon(\omega)=\varepsilon_1(\omega)+i\varepsilon_2(\omega)$, which is mostly associated with the electronic structures. Characterizing the behavior of materials to incident solar radiations is a crucial factor to consider. Furthermore, the static dielectric constant, which refers to the dielectric function at zero photon energy, holds significant importance as a material parameter in optoelectronic

Technium Vol. 13, pp.88-101 (2023)
ISSN: 2668-778X
www.techniumscience.com

applications. The enhancement of device performance and reduction of charge carrier recombination can be attributed to the presence of a high dielectric constant [27-29]. The calculation of the imaginary component $\varepsilon_2(\omega)$ of the dielectric function $\varepsilon(\omega)$ involves evaluating the momentum matrix elements between the occupied and unoccupied states while adhering to the selection rules and given by:

$$\varepsilon_2\omega = \frac{2e^2\pi}{\Omega\varepsilon_0}\sum_{k,v,c} \Psi_k^c \hat{u}.r\Psi_k^{v\,2}\delta E_k^c - E_k^c - E$$

where ω represents the frequency of light, e refer to the charge of electron, ψ_k^c and ψ_k^γ are the CB and VB wave-functions, respectively. The real part of $\varepsilon(\omega)$ can be obtained through the use of the Kramers-Kronig equation, which relates it to $\varepsilon_2(\omega)$. And for other optical constant which depend on absorption spectrum can be derived from the real and imagery dielectric parts [30-32]. The $\varepsilon_1(\omega)$ for $LiNbO_3$ as a function of photon energy is shown in Fig. 3, the pure $LiNbO_3$ possesses semiconducting properties for energy ranges for which $\varepsilon_1(\omega) > 0$. For the real part of $\varepsilon(\omega)$, the highest peak for pure $LiNbO_3$ appears at around 3.75 eV, and we observed its reduce to 2.5 eV for doped $LiNbO_3$ by MO (I) and MO (II) respectively. On the other hand, the imaginary component $\varepsilon_2(\omega)$ indicates its first peak at 4.12 eV for pure crystal and 3.5 eV , 2.9 eV for $LiNbO_3$ doped by MO (I) and MO (II) respectively.

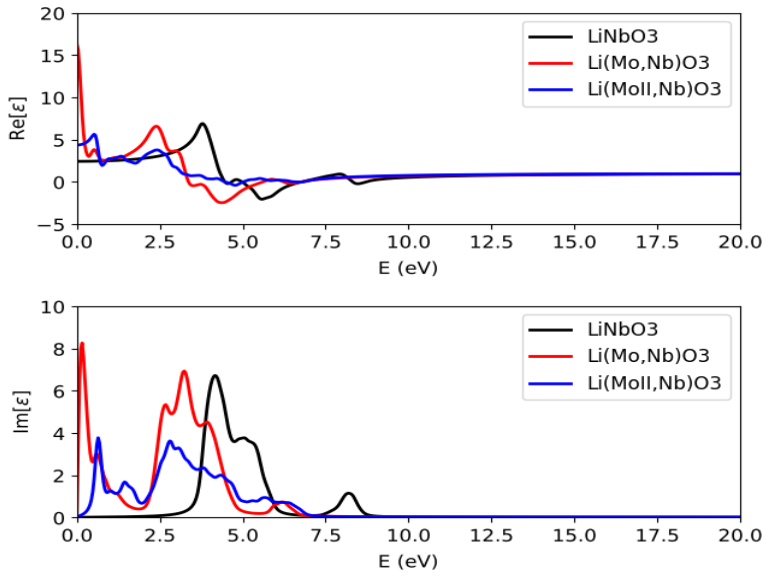

Figure 3. Dielectric constant as a function to energy gap (eV) of $LiNbO_3$ and doped $LiNbO_3$ by Mo (I) and Mo (II) respectively.

Fig. 4 shows the absorption coefficient of $LiNbO_3$ and doped $LiNbO_3$ by Mo (I) and Mo (II) respectively. The absorption coefficient for pure $LiNbO_3$ appears as two peak the first in 170 nm and

the second and highest is about 220 nm, we can noticed the doping by Mo (I) caused little bit decrease in peak absorption and its easy to noticed the peak become more broad, with the absorption range from 200 nm to 580 nm. This effect consider as important to an applications looking for wide range absorption materials such as solar cell applications [33, 34]. While we find the doping by Mo (II) caused decreased in the absorption amplitude to the half of pure $LiNbO_3$ absorption value. And also the absorption peak become broader to the 200-600 nm range.

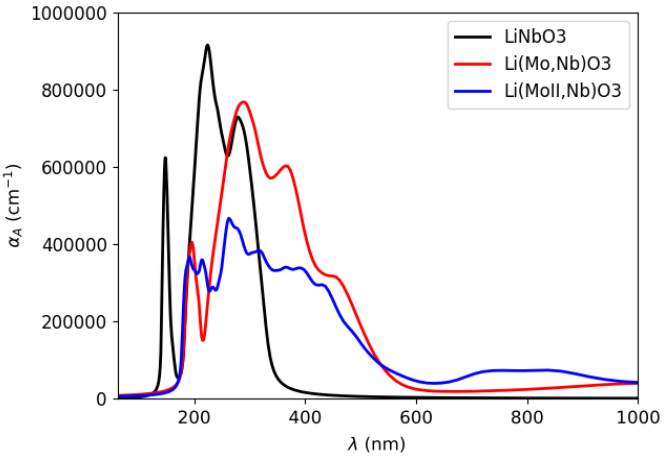

Figure 4. The Absorption coefficient of $LiNbO_3$ and doped $LiNbO_3$ by Mo (I) and Mo (II) respectively.

The refractive index is a dimensionless number that characterizes the speed of light passing through the material and its transparency to photons. To measure the pure and doped $LiNbO_3$ transparency to incident light we present the refractive index and reflectivity spectrum as a function of energy in eV in Fig. 5, and 6, respectively. The static refractive index n(0) it's a valuable constant for many applications, was found to be 1.6 , 4, and 2.1 respectively, of $LiNbO_3$ and doped $LiNbO_3$ by Mo (I) and Mo (II) respectively. Which is consistent with other reported experimental and theoretical values [35-37]. In addition, the refractive index value decrease for photon energies great than 2.5 eV for doped $LiNbO_3$ by Mo (I) and Mo (II). And its decrease after 4 eV for pure $LiNbO_3$. The result showed the Pure and doped $LiNbO_3$ have a different values for refractive index and the maximum value from 2.5-4 eV for of $LiNbO_3$ and doped $LiNbO_3$ by Mo (I) and Mo (II) respectively. And the range from 2.5- 5.5 eV for pure $LiNbO_3$.

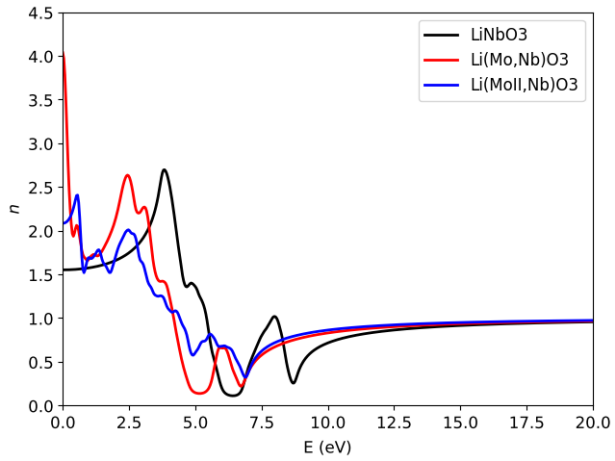

Figure 5. The reflective index of $LiNbO_3$ and doped $LiNbO_3$ by Mo (I) and Mo (II) respectively.

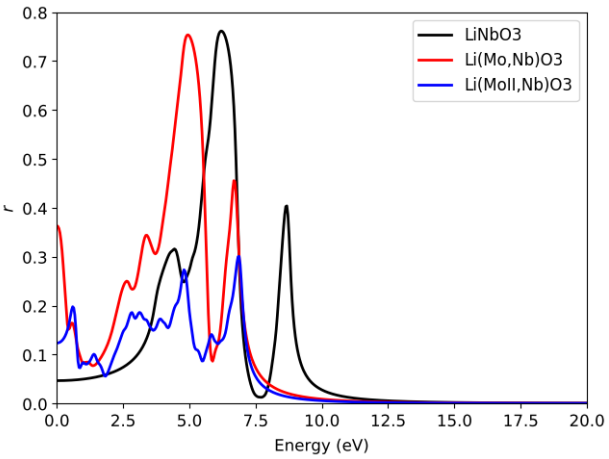

Figure 6. The reflectivity spectrum of $LiNbO_3$ and doped $LiNbO_3$ by Mo (I) and Mo (II) respectively.

Extinction coefficient (k) refers to several different measures of the absorption of light in a medium. It is commonly referred to as the imaginary component of the refractive index, which governs the level of attenuation experienced by an electromagnetic wave as it travels through a material. And k is equal to zero at (0) photon energy for three structures as shown in Fig 7.

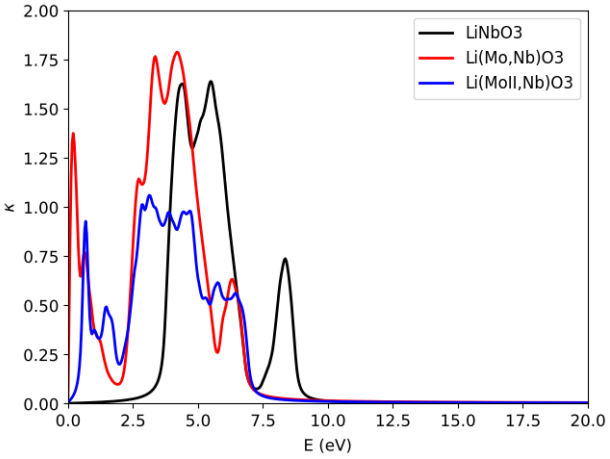

Figure 7. Extinction constant as a function to energy gap (eV) of $LiNbO_3$ and doped $LiNbO_3$ by Mo (I) and Mo (II) respectively.

Second harmonic generation (SHG) one of a strong nonlinear optical (NLO) responses. Its represent a special case of sum frequency generation. This effect play a role for many photonic applications such as laser applications, electro optics, and optical switches [38-40]. So the search about materials with the noncentrosymmetric and large SHG effect it has attracted the attention of researchers for last decades. In this paper, we looking to enhance the SHG effect for $LiNbO_3$ crystal by doping strategy. The doping process done with Mo (I) and Mo (II) respectively and we compare the SHG results with a pure $LiNbO_3$ crystal which it's present in Fig. 8 (a, b, c0 respectively. The pure crystal result shows a maximum peak at 4 eV and small peak at 2.2 eV. The doping by Mo (II) shows increase by peak value Ten times more from pure crystal approximately and a peak shift to low photon energy estimated at 3 eV approx.

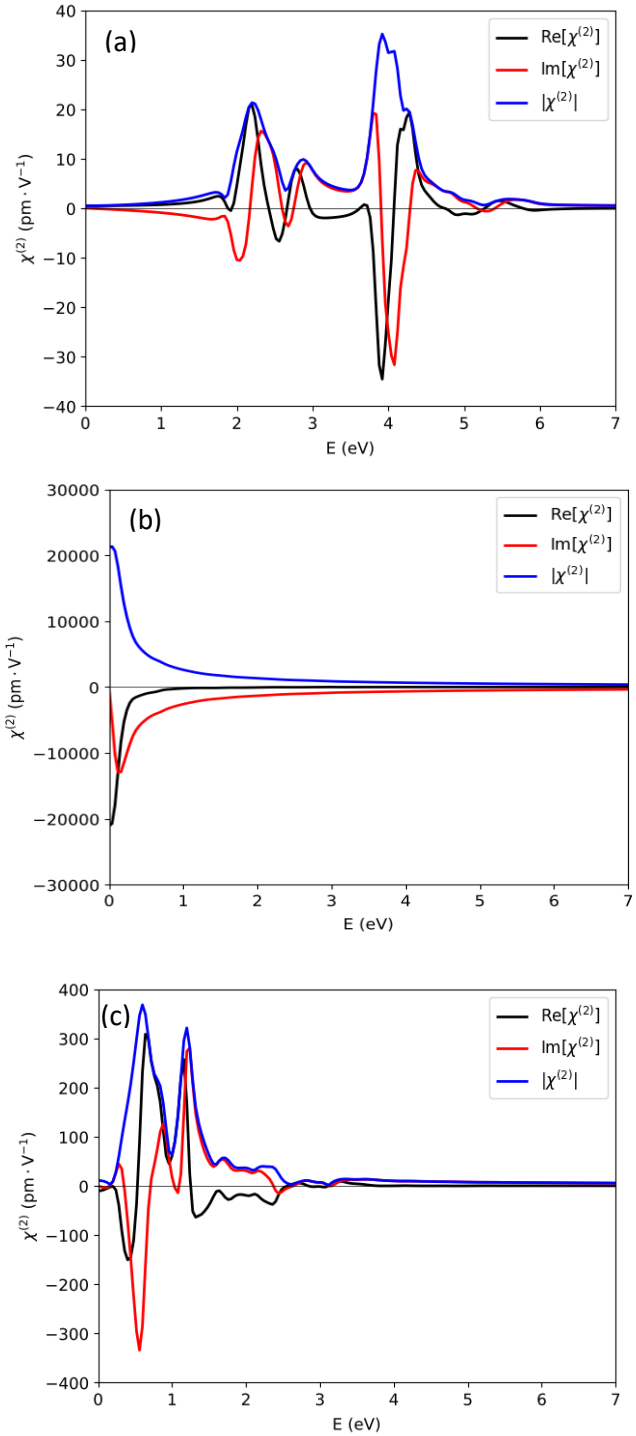

Figure 8. The reflectivity spectrum of (a) $LiNbO_3$ and doped $LiNbO_3$ by (b) Mo (I) and (c) Mo (II) respectively.

Conclusions

This study focuses on the Mo-Nb doped $LiNbO_3$ system, specifically examining the effects of Mo (I) and Mo (II) doping. These doping are denoted as Li(Nb, Mo I)O_3 and Li(Nb, Mo II)O_3, respectively. The present study used first-principles computations to analyze the electronic and optical characteristics of Mo-doped $LiNbO_3$ systems, with a comparison made to the pure $LiNbO_3$ material. The results of the DFT calculations indicate a clear distinction in the electronic characteristics of $LiNbO_3$, Li(Nb, Mo I)O_3, and Li(Nb, Mo II)O_3. The band structures that have been computed indicate that Li(Nb, Mo I)O_3 possesses a relatively narrow band gap of 2.068 eV, while Li(Nb, Mo II)O_3 exhibits an even lower band gap of 0.476 eV. It is noteworthy that the band gap of Li(Nb, Mo II)O_3 is smaller than that of pure $LiNbO_3$, which has a band gap of 3.538 eV. The optical results show an interesting UV-V is spectrum for the doped $LiNbO_3$ by (Mo I) and (Mo II) the effect of doping with these elements led to obtaining an absorption spectrum with a wider bandwidth than that of pure crystal. This in turn is an important result for many applications that require a broad absorption spectrum.

References

[1] M. Jazbinsek, L. Mutter, and P. Gunter. (2008). Photonic applications with the organic nonlinear optical crystal DAST. *IEEE Journal of selected topics in quantum electronics*, *14*(5), 1298-1311.

[2] L. R. Dalton, P. A. Sullivan, and D. H. Bale. (2010). Electric field poled organic electro-optic materials: state of the art and future prospects. *Chemical reviews*, *110*(1), 25-55.

[3] C. Sanchez, B. Lebeau, F. Chaput, and J. P. Boilot. (2003). Optical properties of functional hybrid organic–inorganic nanocomposites. *Advanced Materials*, *15*(23), 1969-1994.

[4] R. Turner, P. A. Fuierer, R. Newnham, and T. R. Shrout. (1994). Materials for high temperature acoustic and vibration sensors: A review. *Applied acoustics*, *41*(4), 299-324.

[5] J. V. Vidal *et al.* (2019). Low-frequency vibration energy harvesting with bidomain LiNbO 3 single crystals. *IEEE Transactions on Ultrasonics, Ferroelectrics, and Frequency Control*, *66*(9), 1480-1487.

[6] R. Weis and T. Gaylord. (1985). Lithium niobate: Summary of physical properties and crystal structure. *Applied Physics A*, *37*, 191-203.

[7] G. Clementi *et al.* (2021). LiNbO3 films–A low-cost alternative lead-free piezoelectric material for vibrational energy harvesters. *Mechanical Systems and Signal Processing*, *149*, 107171.

[8] A. Abdollahi, Z. Jiang, and S. A. Arabshahi. (2007). Evaluation on mass sensitivity of SAW sensors for different piezoelectric materials using finite-element analysis. *IEEE transactions on ultrasonics, ferroelectrics, and frequency control*, *54*(12), 2446-2455.

[9] D. A. Scrymgeour and V. Gopalan. (2005). Nanoscale piezoelectric response across a single antiparallel ferroelectric domain wall. *Physical Review B*, *72*(2), 024103.

[10] D. Zhu *et al.* (2021). Integrated photonics on thin-film lithium niobate. *Advances in Optics and Photonics*, *13*(2), 242-352.

[11] Y. Jia *et al.* (2022). Integrated Photonics Based on Rare-Earth Ion-Doped Thin-Film Lithium Niobate. *Laser & Photonics Reviews*, *16*(9), 2200059.

[12] A. Boes, B. Corcoran, L. Chang, J. Bowers, and A. Mitchell. (2018). Status and potential of lithium niobate on insulator (LNOI) for photonic integrated circuits. *Laser & Photonics Reviews*, *12*(4), 1700256.

[13] L. Eldada. (2004). Optical communication components. *Review of Scientific Instruments*, *75*(3), 575-593.

[14] K. Stokbro, J. Taylor, M. Brandbyge, and P. Ordejon. (2003). TranSIESTA: a spice for molecular electronics. *Annals of the New York Academy of Sciences*, *1006*(1), 212-226.

[15] J. M. Soler *et al.* (2002). The SIESTA method for ab initio order-N materials simulation. *Journal of Physics: Condensed Matter*, *14*(11), 2745.

[16] J. P. Perdew, K. Burke, and M. Ernzerhof. (1996). Generalized gradient approximation made simple. *Physical review letters*, *77*(18), 3865.

[17] H. J. Monkhorst and J. D. Pack. (1976). Special points for Brillouin-zone integrations. *Physical review B*, *13*(12), 5188.

[18] J. Yu and X. Liu. (2007). Hydrothermal synthesis and characterization of LiNbO3 crystal. *Materials Letters*, *61*(2), 355-358.

[19] M. M. Hossain. (2019). First-principles study on the structural, elastic, electronic and optical properties of LiNbO3. *Heliyon*, *5*(4).

[20] W. Abdul-Hussein, F. H. Hanoon, and L. F. Al-Badry. (2023). Control the electronic and optical properties of AlN nanosheet by the electric field. *Results in Optics*, *11*, 100423.

[21] A. Dhar and A. Mansingh. (1990). Optical properties of reduced lithium niobate single crystals. *Journal of applied physics*, *68*(11), 5804-5809.

[22] C. Thierfelder, S. Sanna, A. Schindlmayr, and W. G. Schmidt. (2010). Do we know the band gap of lithium niobate? *physica status solidi c*, *7*(2), 362-365.

[23] H. Xu *et al.* (2008). Stability of intrinsic defects and defect clusters in Li Nb O 3 from density functional theory calculations. *Physical Review B*, *78*(17), 174103.

[24] M. K. Shahzad *et al.* (2022). Zirconium-based cubic-perovskite materials for photocatalytic solar cell applications: a DFT study. *RSC advances*, *12*(42), 27517-27524.

[25] J. U. Rehman *et al.* (2022). First-principles calculations to investigate structural, electronics, optical and elastic properties of Sn-based inorganic Halide-perovskites CsSnX3 (X= I, Br, Cl) for solar cell applications. *Computational and Theoretical Chemistry*, *1209*, 113624.

[26] B. Dai *et al.* (2021). Piezo-phototronic effect on photocatalysis, solar cells, photodetectors and light-emitting diodes. *Chemical Society Reviews*, *50*(24), 13646-13691.

[27] X.-Z. Zhang, K.-S. Shen, Z.-Y. Jiao, and X.-F. Huang. (2013). A study of the electronic structures and optical properties of CuXTe2 (X= Al, Ga, In) ternary semiconductors. *Computational and Theoretical Chemistry*, *1010*, 67-72.

[28] A. Amudhavalli, R. Rajeswarapalanichamy, K. Iyakutti, and A. Kushwaha. (2018). First principles study of structural and optoelectronic properties of Li based half Heusler alloys. *Computational Condensed Matter*, *14*, 55-66.

[29] F. M. Hossain, L. Sheppard, J. Nowotny, and G. E. Murch. (2008). Optical properties of anatase and rutile titanium dioxide: Ab initio calculations for pure and anion-doped material. *Journal of Physics and Chemistry of Solids*, *69*(7), 1820-1828.

[30] J. Liu and E. Hua. (2015). Electronic structure and absolute band edge position of tetragonal AgInS2 photocatalyst: A hybrid density functional study. *Materials Science in Semiconductor Processing*, *40*, 446-452.

[31] C. Li, B. Wang, R. Wang, H. Wang, and X. Lu. (2008). First-principles study of structural, elastic, electronic, and optical properties of orthorhombic BiGaO3. *Computational Materials Science*, *42*(4), 614-618.

[32] M. Hasan and A. A. Hossain. (2022). First-principles calculations to investigate the structural, electronic, optical anisotropy, and bonding properties of a newly synthesized ThRhGe equiatomic ternary intermetallic superconductor. *Results in Physics*, *42*, 106004.

[33] Y. Li. (2012). Molecular design of photovoltaic materials for polymer solar cells: toward suitable electronic energy levels and broad absorption. *Accounts of chemical research*, *45*(5), 723-733.

[34] Y.-J. Cheng, S.-H. Yang, and C.-S. Hsu. (2009). Synthesis of conjugated polymers for organic solar cell applications. *Chemical reviews*, *109*(11), 5868-5923.

[35] L. Arizmendi. (2004). Photonic applications of lithium niobate crystals. *physica status solidi (a)*, *201*(2), 253-283.

[36] Y. Qi and Y. Li. (2020). Integrated lithium niobate photonics. *Nanophotonics*, *9*(6), 1287-1320.

[37] M. Veithen, X. Gonze, and P. Ghosez. (2004). First-principles study of the electro-optic effect in ferroelectric oxides. *Physical review letters*, *93*(18), 187401.

[38] D. Arivuoli. (2001). Fundamentals of nonlinear optical materials. *Pramana*, *57*, 871-883.

[39] Y. Zhou, Y. Huang, X. Xu, Z. Fan, J. B. Khurgin, and Q. Xiong. (2020). Nonlinear optical properties of halide perovskites and their applications. *Applied Physics Reviews*, *7*(4).

[40] S. Semin, X. Li, Y. Duan, and T. Rasing. (2021). Nonlinear optical properties and applications of fluorenone molecular materials. *Advanced Optical Materials*, *9*(23), 2100327.